Research Article

Yang Wen, Hui Sun*, Shuaidong Hu, Guangmao Xu, Xiazhi Wu, Congcong Song, Zhen Liu, and Zhaojian Li

# Microstructure and life prediction model of steel slag concrete under freezing-thawing environment

https://doi.org/10.1515/ntrev-2021-0109
received September 3, 2021; accepted October 16, 2021

**Abstract:** The goals of this paper are to study the frost resistance of steel slag concrete (SSC), research the damage mechanisms, and predict the service life of SSC in cold regions. First, the stability of steel slag (SS) was tested, and then SS samples with different treatment dosages were used as aggregates to replace natural aggregates of equal volumes in the preparation of C40 concrete. The microstructures of concrete and micro properties of cement hydration products were investigated in nanospace in this research. In addition, rapid frost resistance durability tests were carried out under laboratory conditions. The results revealed that the ordinary concrete (OC) exhibited a more serious damage phenomenon, and the mass loss and relative dynamic elastic modulus of OC were changed by 5.27 and 62.30%, respectively. However, with increases in the SS content, the losses in mass were lowered. Furthermore, the relative dynamic elastic modulus decreased less, and the frost resistance of the specimens was stronger. The range of mass loss rate was between 2.233 and 3.024%, and the relative dynamic elastic modulus range was between 74.92 and 91.09%. A quadratic function with a good fitting degree was selected to establish a freezing-thawing damage calculation model by taking the relative dynamic elastic modulus as the variable. Then, the freezing-thawing durability lifespan of concrete in the colder regions of northern China was successfully predicted by using the damage calculation model. The results of $SSC_{20-60}$ showed the better frost resistance durability when the content of SS sand was 20% and the dosage of SS stone was 60%. Its frost resistance lifespan was more than twice that of OC, which demonstrated that SS as an aggregate could effectively improve the frost resistance lifespan of concrete to a certain extent.

**Keywords:** steel slag concrete, microstructure, freezing-thawing damage model

## 1 Introduction

In the process of steel production, the United States geological survey estimated in 2015 that the amount of SS produce yearly would be about 170–250 million metric tons, and that China could produce about 120 million tons of SS in one year [1,2]. Great amounts of SS have been disposed as waste, which in turn results in the waste of resources and environmental pollution. Therefore, using and recycling of SS from the steel manufacturing industry is an important issue and it is urgent that we take effective measures to apply SS to concrete, which is of great significance for conserving resources and building a green and environmental protection environment.

At the present time, researchers had completed a large number of experimental studies regarding the properties of steel slag concrete (SSC) [3–8], and most of these experiments have included investigating the compressive strength, tensile and flexural strength, the bulk density, and so on. Subathra Devi and Gnanavel [9] studied the properties of concrete manufactured using SS; the results showed that for conventional concrete, the partial replacement of fine and coarse aggregates by SS improved the compressive, tensile, and flexural strength. Chunlin *et al.* [10] researched the possibility of concrete prepared with SS as fine and coarse aggregates, volume deformation, compressive and flexural strength of concrete containing SS, and (or) scrap tire particles as aggregate were experimentally investigated by strength test; the results indicated that the mechanical strength of SSC was acceptable,

* **Corresponding author: Hui Sun,** School of Civil Engineering, Inner Mongolia University of Science and Technology, Baotou, Inner Mongolia, 014010, China, e-mail: 1226186340@qq.com
**Yang Wen, Shuaidong Hu, Guangmao Xu, Xiazhi Wu, Congcong Song, Zhen Liu, Zhaojian Li:** School of Civil Engineering, Inner Mongolia University of Science and Technology, Baotou, Inner Mongolia, 014010, China

**Table 1:** Physical performance indexes of cement

| Fineness [80 μm] (%) | Specific surface area ($m^2$/kg) | Setting time (min) | | Flexural and compressive strength (MPa) | |
|---|---|---|---|---|---|
| | | Initial setting | Final setting | 3 days | 28 days |
| 3.3 | 341 | 130 | 226 | 5.6/25.2 | 8.9/49.2 |

though slightly lower flexural strength than that of conventional was noticed. Wang used SS to replace natural aggregate in pervious concretes (PCs) and researched the properties of the PCs, including the compressive strength, the splitting tensile strength and the flexural strength as well as the bulk density; the connected porosity and the water permeability coefficient were studied. In general, steel slag (SS) can be used as alternative aggregate to replace natural aggregate in preparing PCs [11]. However, most of the existing research studies have only focused on the basic properties of SSC and less on the frost resistance of SSC. Under the circumstance of cold regions, the concrete would bear the freezing-thawing damage, thereby reducing the service life of concrete. Therefore, the research on frost resistance of SSC is of great significance to solve the frost-resisting durability of concrete structures in cold regions.

In order to solve the freezing-thawing damage problems of concrete and increase the service life of concrete structures in severe cold regions, SS was used to replace natural aggregate into C40 concrete in this work. The replacement levels of SS were 20, 40, and 60%, respectively. Relative dynamic elastic modulus loss rates have been widely used due to the ease of achieving nondestructive testing results [12–20] and the relative dynamic elastic modulus damage model of concrete established by Sun *et al*. [21] has been confirmed to achieve a good fitting accuracy. Therefore, the freezing-thawing damage model was established by using the relative dynamic elasticity as a variable to predict service life under cold conditions in various regions of the north. In addition, the microstructure of concrete and properties of hydration products were also investigated in nanospace in this research, combined with micro and macro physical phenomena, and the causes of their superior frost resistance of SSC were comprehensively analyzed. Therefore, these results in this work would be of great significance to provide reference and predict the damage degree of SSC serving in cold regions in the future.

**Table 2:** Physical properties of fly ash

| Apparent density ($kg/m^3$) | Water demand ratio (%) | 45 μm fineness (%) | Activity index (%) | | |
|---|---|---|---|---|---|
| | | | 3 days | 7 days | 28 days |
| 2,300 | 99 | 19.4 | 59.1 | 63.3 | 82.4 |

# 2 Experimental overview

## 2.1 Raw materials

The P·O 42.5 grade Ordinary Portland cement applied in this study was produced by the Jidong Cement Company. The concrete's main physical performance indicators are shown in Table 1.

The fly ash utilized in this research investigation was produced by the Hexi Power Plant in Baotou City, and its physical properties are detailed in Table 2.

The natural aggregate was selected from Baotou City. The fineness modulus of the sand was 2.9, and the particle sizes of the stone ranged from 5 to 25 mm. The physical performance indicators are outlined in Table 3.

**Admixture:** The water reducing rate of polycarboxylate superplasticizers can reach 30%. This study's testing results also conformed to the GB 8076-2008 "concrete admixture."

SS stone with particle sizes ranging between 5 and 25 mm, and SS with particle sizes less than 5 mm, is selected as the sand component in this study. The

**Table 3:** Physical properties of natural aggregate

| Category | Apparent density ($kg/m^3$) | Bulk density ($kg/m^3$) | Water content (%) | Soil content (%) | Water absorption (%) |
|---|---|---|---|---|---|
| Sand | 2,600 | 1,620 | 1.4 | 1.7 | 0.9 |
| Stone | 2,750 | 1,470 | 0.3 | 0.7 | 0.8 |

**Table 4:** Physical properties of SSA

| Category | Apparent density (kg/m$^3$) | Bulk density (kg/m$^3$) | Water content (%) | Soil content (%) | Water absorption (%) |
|---|---|---|---|---|---|
| SS sand | 3,520 | 2,110 | 0.25 | 0.2 | 4.3 |
| SS stone | 3,560 | 1,820 | 0.20 | 0.18 | 3.5 |

physical properties of steel slag aggregate (SSA) are detailed in Table 4.

The SS stone is shown in Figure 1(a). It can be seen in the figure that the appearance was grayish and light brown. The surfaces were rough and irregular with small holes observed. The SS sand and internal appearances are shown in Figure 1(b) and (c). As shown in the figure, the appearance characteristics exhibited gray-black coloration, and the internal appearance was scanned using an electron microscope. There were a large number of internal holes observed which ranged between 10 and 100 μm, and the surface areas were irregular.

In the present investigation, the chemical composition of the SS was analyzed using X-ray fluorescence spectroscopy. The specific composition is detailed in Table 5. The main chemical composition of the SS was similar to that of Portland cement clinker, and it displayed certain cementitious properties. However, when compared with cement clinker, the SSA contained higher iron content, which helped improve such physical properties of the concrete as shrinkage and frost resistance.

The alkalinity coefficient calculated according to the chemical composition of the SS could then be used to measure the activities. The definition of SS alkalinity in China adopts the method of Mason B [22], in which the alkalinity value can be measured in formula (1).

$$R = \omega(\mathrm{CaO})/\omega(\mathrm{SiO_2} + \mathrm{P_2O_5}), \quad (1)$$

where $R$ represents alkalinity value (%), $\omega$ indicates the content of chemical components (%).

The alkalinity of the SS in this study was determined to be 2.4%, or in the medium alkalinity range. Therefore, the activity of the SS was considered to be good.

The results of this study's X-ray analysis are shown in Figure 2. The SS contained mineral components such as $C_3S$, $C_2S$, $C_2F$, RO phase (FeO, MnO, MgO, and other solid solutions), and small amounts of residual steel. The silicate minerals were found to be helpful in improving the activity of the SS, as well as the interface properties between the aggregate and the cement. It is known that the RO phase directly affects the stability of SS. SS contains some minerals, such as olivine and rose pyroxene, which makes the wear resistance of SS better than that of ordinary gravel. Therefore, it is considered to be feasible to replace natural aggregates with SS.

## 2.2 Mixture proportion

The mix proportions of the C40 ordinary concrete (OC) utilized in this study were designed according to JGJ 55-2011 "Specification for mix proportion design of OC."


**Figure 1:** The appearance of SS: (a) SS stone; (b) SS sand; and (c) internal appearance.

**Table 5:** Chemical composition of SSA

| Composition | CaO | MgO | $Fe_2O_3$ | $Al_2O_3$ | $SiO_2$ | F-CaO | Other |
|---|---|---|---|---|---|---|---|
| Mass fraction (%) | 38.89 | 12.14 | 25.28 | 2.70 | 16.20 | 0.64 | 4.15 |

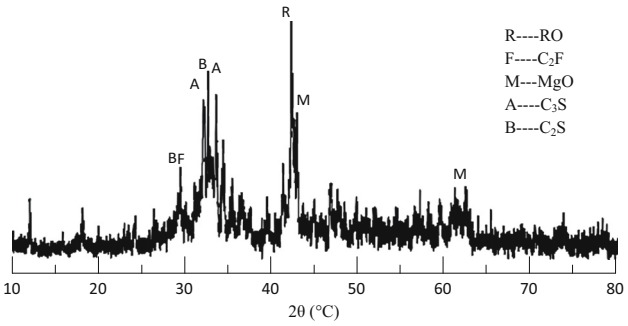


**Figure 2:** XRD pattern of SSA.

Also, the SS was mixed using various proportions. Finally, five groups of SSC with the best content characteristics were selected. The specific mix proportions are detailed in Table 6.

## 2.3 Test method

### 2.3.1 SS stability test

For the SS stability test, the GB/T24175-2009 "SS stability test method" was referred to, a YZF-2S cement autoclave machine was used to carry out the test, and the stability of the SS was determined by measuring the autoclaved pulverization rates. The principle was that the free CaO and MgO in the SS were autoclaved under 2.0 MPa saturated steam. The stability of the SS was determined by measuring the sizes of the SS digestion pulverization rates. The smaller the rate was, the better the stability of the SS would be.

The experimental steps were as follows:

(1) First, 10 kg SS stone was selected in the 5–25 mm particle size range and completely broken; then crushed through a 9.5 mm square pore sieve; placed in a 105 ± 5°C oven for drying; cooled; and passed through a secondary 4.75 mm square pore sieve screen. Three samples of 800 g were weighed in a 4.75–9.5 mm residue. Then, 10 kg SS sand with particle sizes less than 4.75 mm was selected; oven-dried and cooled; and passed through a 2.36 mm square pore sieve. Samples measuring 2.36–4.75 mm were selected, and three 800 g samples were weighed.

(2) After all of the samples had been washed, they were placed into an autoclave for 3 h. Then, the samples were removed and dried after cooling; weighed; denoted as $m_0$; passed through a 1.18 mm sieve; and weighed as $m_1$. The pulverization rate formula was as follows:

**Table 6:** Concrete mix ratio (kg/m$^3$)

| Number | Cement | Fly ash | Fine aggregate | | Coarse aggregate | | Water | Admixture |
|---|---|---|---|---|---|---|---|---|
| [a]C | 280 | 120 | 768.6 | 0 | 1061.4 | 0 | 170 | 6 |
| $SSC_{20-20}$ | 280 | 120 | 556.3 | 182 | 907.7 | 280.9 | 170 | 6 |
| [b]$SSC_{20-40}$ | 280 | 120 | 556.3 | 182 | 680.8 | 561.9 | 170 | 6 |
| $SSC_{20-60}$ | 280 | 120 | 556.3 | 182 | 453.8 | 842.8 | 170 | 6 |
| $SSC_{40-20}$ | 280 | 120 | 417.2 | 364 | 907.7 | 280.9 | 170 | 6 |
| $SSC_{60-20}$ | 280 | 120 | 278.2 | 546 | 907.7 | 280.9 | 170 | 6 |

[a]C: Ordinary concrete.
[b]$SSC_{20-40}$: Steel slag concrete with 20% steel slag sand and 40% steel slag stone.

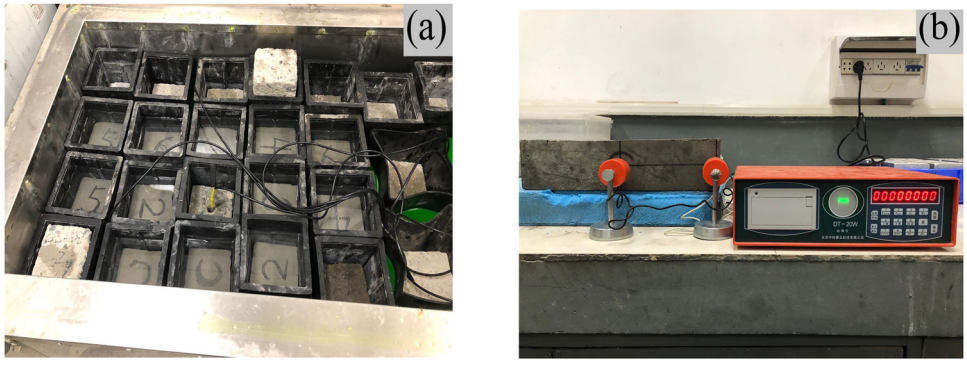


**Figure 3:** (a) Freezing-thawing specimens and (b) measurement of relative dynamic elastic modulus.

$$f = \frac{m_1}{m_0} \times 100\%, \quad (2)$$

where $f$ represents pulverization rate (%), $m_0$ indicates the mass of samples after test (g), $m_1$ indicates the mass of samples after passing 1.18 mm sieve (g).

(3) Test results: The average autoclaved pulverization rates of the fractions were 3.31 and 3.55%, respectively. In addition, with references made to YB/T 4201-2009 "SS sand for ordinary ready-mixed mortar" and YB/T 4329-2012 "Application Technology of SS Sand for Cement Concrete Pavement," both were within 5.9%, which met the requirements of this study.

#### 2.3.2 Freezing-thawing test

The freezing-thawing parameters were tested according to the GB/T 50082-2009 "Standard for test methods of the long-term performance and durability of OC." An IMDR concrete rapid freezing-thawing machine was used to carry out the freezing-thawing cycle test of the concrete. Specimens in the size range of 100 mm × 100 mm × 400 mm were designed using a fast-freezing method. After 24 days, the specimens were immersed in water at approximately 20°C, then removed after 4 days, and the surface moisture was wiped dry. Prior to testing, the water was required to pass the upper surfaces of the specimens and exceed 5 mm, as shown in Figure 3(a). The freezing-thawing test set 150 cycles. The mass losses and relative dynamic elastic modulus were tested every 25 cycles. The determination of the elastic modulus is shown in Figure 3(b). The testing process could be stopped if one of the following conditions occurs: (1) The freezing-thawing cycles reached a specified number; (2) The relative dynamic modulus of elasticity decreased to 60%; (3) The mass loss rate reached 5%.

## 3 Results and analysis

### 3.1 Experimental phenomena

The failure phenomena observed in this study are shown in Figure 4. From left to right in the figure, (according to the number of freezing-thawing cycles) the observations followed 0, 50, 100, and 150 cycles. It was found that the surfaces of the specimens prior to testing were complete and smooth, and there was dense cement slurry wrapped on the outside. However, when the specimens were removed after the 50th cycle, the cement mortar epidermis outside the OC had begun to fall off. The main reason for this was that, with the increase of freezing-thawing cycles, the micro pores on the surface of OC continued to develop and were converted to large holes, so that the surface of OC was seriously damaged [23]. By comparison, the number of holes on the surfaces of SS was fewer in number. The reason for this was that SS could produce C–S–H gels and fill some of the pores, which could effectively prevent the flow of the aqueous solution, and the hydrostatic pressure or osmotic pressure could be reduced, thereby further reducing the degree of freezing-thawing damage in SSC [24]. When the freezing-thawing cycles were carried out to the 100th cycle, the aggregate was found to be exposed, and the OC was observed to be the most severe. This was due to the repeated freezing-thawing of water in the capillary of concrete, which led to the continuous extension and expansion of cracks, and finally led to the mutual penetration of cracks. At the same time, the completely closed microbubbles began to produce frost heave cracking under the effects of expansion pressure stress and osmotic pressure stress, and the network or flocculent C–S–H gels formed by cement hydration began to increase [25]. Meanwhile, the specimens of the $SSC_{20-60}$ group only displayed the phenomenon of cement mortar epidermis shedding. When the freezing-thawing was carried out to the 150th cycle, the specimens were found to be damaged to varying degrees. The damages to the OC were the most serious, with even the aggregate falling off. However, the SSC with different dosages only showed the mortar falling off, with the aggregate remaining intact. The main reason for these results was that with the increase of freezing-thawing cycles, aqueous solution continuously enters the concrete and freezing-thawing occurs in the pores. When the expansion pressure produced by ice crystal exceeded the force that concrete could bear, the surface would exhibit a frost heave cracking phenomenon, and a large number of micro-cracks would form on the surface, resulting in the gradual accumulation of damage [26].

In the present research investigation, a comparison of test phenomena after 150 freezing-thawing cycles was made. It was found that the OC was more seriously damaged when compared with the SSC. However, the SSC only underwent shedding of the outsourcing mortar layers, which indicated that SS as an aggregate mixed with concrete could more effectively resist the damages caused by freezing-thawing cycles. The reason for this was that SS could react to the cement hydration producing C–S–H gels, which would play a good filling role, thereby improving the density of SSC [27], so that the hydrostatic pressure or osmotic pressure could be reduced, which resulted in the overall structure being denser [28].

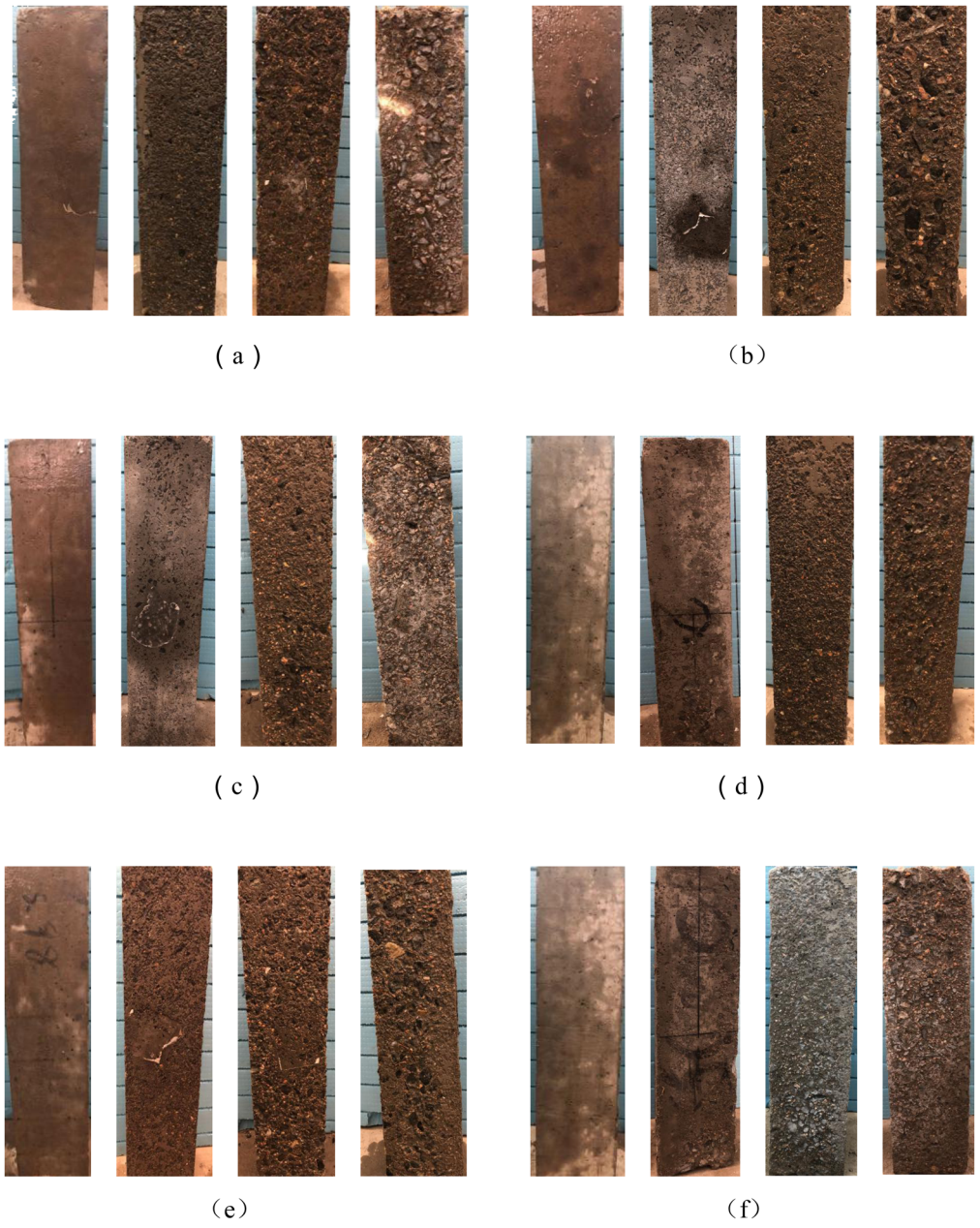


**Figure 4:** Failure characteristics. (a) C, (b) $SSC_{20-20}$, (c) $SSC_{20-40}$, (d) $SSC_{20-60}$, (e) $SSC_{40-20}$, and (f) $SSC_{60-20}$.

In addition, the interfacial transition zone (ITZ) between SS and cement stone was small, which could form strong interfacial adhesion, so that the overall structure was stabler, thereby further reducing the degree of freezing-thawing damage in SSC [29].

## 3.2 Microscopic study

Concrete is a kind of porous material, and through the reaction of water and cement, it will form a hardening slurry which can cement sand and stone together, and the original internal space filled by water will not be fully filled by hydration products, which will become pores. These pores are usually referred to as fine pores, and the pore size is generally several nanometers to several microns, which has an important influence on the frost resistance of concrete [30,31]. Therefore, it is necessary to analyze the microstructure of concrete and properties of hydration products in nanospace. A Sigma500 SEM was used to analyze the broken specimens of OC and $SSC_{20-60}$ in this study; test instruments are shown in Figure 5. The

**Figure 5:** Scanning electron microscope.

transition zones between the aggregate and the cement stone interfaces, along with the hydration products, are shown in Figures 6 and 7.

Figure 6(a) shows that there were obvious micro-cracks about 2 μm wide in the interface transition zone of OC due to the unfavorable bonds between the natural aggregate and the cement paste. With the progress of freezing-thawing cycles, after the aqueous solution entered the concrete, it froze and thawed continuously, and when the expansion pressure generated by ice crystals exceeded the force that the concrete could bear, the performance of the bonding interface between aggregate and cementitious materials in OC would be further seriously damaged [32]. According to the viewpoint of random damage in damage mechanics, the initial damage area of concrete is in ITZ where the connection between crystals can be regarded as a "micro-spring system" [33]. Figure 6(b) shows that the ITZ of $SSC_{20-60}$ were denser due to the close bonds between the SSA and the cement stone. In other words, the number of "micro-springs" was greater. Therefore, when the two were subjected to the same freezing-thawing damage conditions, the degrees of cracking damage of the SSC were lower and the macroscopic freezing-thawing resistance was better than that of the OC specimens.

Figure 7 shows that the hydration products in the ITZ were mainly coral-like C–S–H gels. It can be seen that the aggregate in Figure 7(a) is surrounded by fibrous and coralline gels which are not sufficiently bound. Besides, with the increase of the freezing-thawing cycles, $SO_4^{2-}$ and the $Ca(OH)_2$ in the cement stone reacted to generate $CaSO_4$, and the $CaSO_4$ would react with hydrated calcium aluminate in cement to generate calcium trisulphoaluminate hydrate (AFt), then the AFt would generate great stress; when the generated stress exceeded the bearing capacity of concrete, the internal micro-cracks of concrete specimens would increase and further develop [34–36]. The chemical composition of the SS was similar to that of the cement. Hydration reaction of dicalcium silicate and tricalcium silicate occurred in a later period, and the chemical reaction can be found in formulas (3) and (4). More gels were produced when hydration occurred during the later period, as illustrated in Figure 7(b). There were holes on the surfaces of the SS which allowed the gels and aggregate to be more closely embedded. At the same time, this had also reduced the number of pores and effectively prevented the flow of the aqueous solution [37].

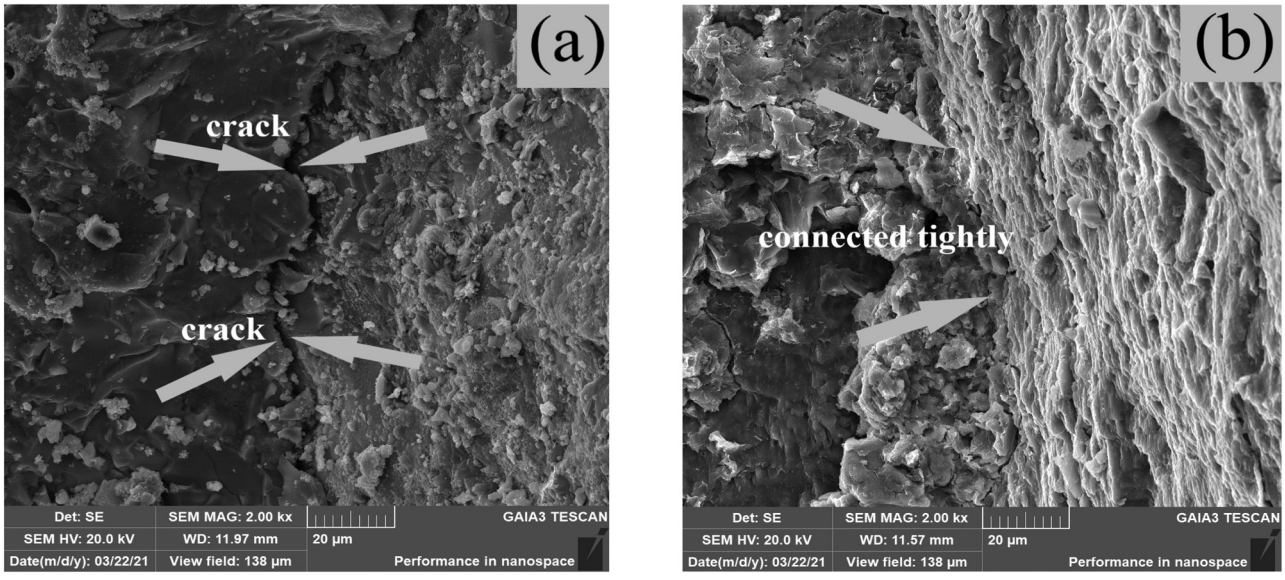


**Figure 6:** ITZ: (a) C and (b) $SSC_{20-60}$.

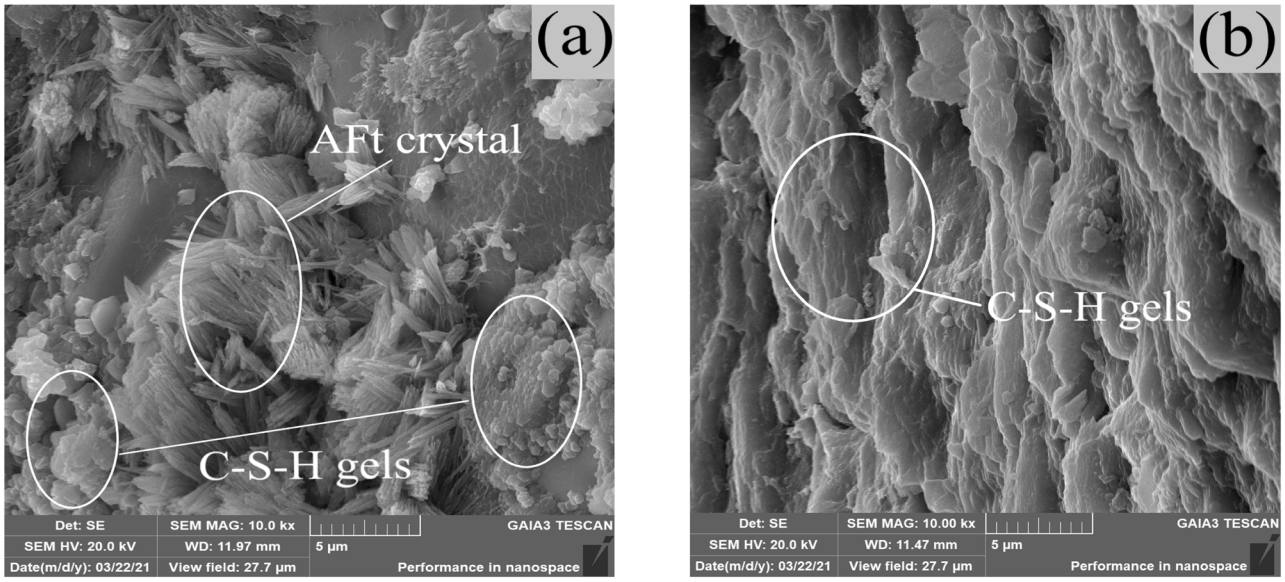


**Figure 7:** Hydration products: (a) C and (b) $SSC_{20-60}$.

Then, hydrostatic pressure or osmotic pressure could be reduced [38], which resulted in the overall structure being more stable and the frost resistance of the SSC being improved.

$$2CaO \cdot SiO_2 + nH_2O = xCaO \cdot SiO_2 \cdot yH_2O + (2 - x)Ca(OH)_2, \quad (3)$$

$$3CaO \cdot SiO_2 + nH_2O = xCaO \cdot SiO_2 \cdot yH_2O + (3 - x)Ca(OH)_2. \quad (4)$$

## 3.3 Freeze-thaw resistance

### 3.3.1 Mass loss

Mass loss rates are important reference factors in the study of concrete freeze-thaw damages; the mass loss rate of concrete specimen after freezing-thawing is calculated according to formula (5). The average value of each group was taken as the final mass loss rate.

$$\Delta Wn = \frac{G_0 - G_n}{G_0} \times 100\%, \quad (5)$$

where $G_0$ represents the mass of concrete specimens before freezing-thawing cycles, $G_n$ indicates the mass of concrete specimens after $N$ times of freezing-thawing cycles.

Figure 8 shows the mass loss rates of the concrete after 0, 50, 100, and 150 freeze-thaw cycles. At the early stage of the freezing-thawing, the folding lines were all relatively gentle. The main reason for this was that the concrete had been soaked before the freeze-thaw cycles and reached the state of water absorption saturation in theory. Therefore, the mass losses were not obvious at the beginning of the freeze-thaw cycles [39]. When the freeze-thaw tests were carried out to the middle and late stages, the loss rates of each group were found to be significantly higher, which corresponded to the observed appearances of the specimens. This was due to the fact that with the increases of the freezing-thawing cycles, $SO_4^{2-}$ and the $Ca(OH)_2$ in the cement stone reacted to generate $CaSO_4$, and the $CaSO_4$ would react with hydrated calcium aluminate to generate AFt, then the AFt would generate great stress; when the generated stress exceeded

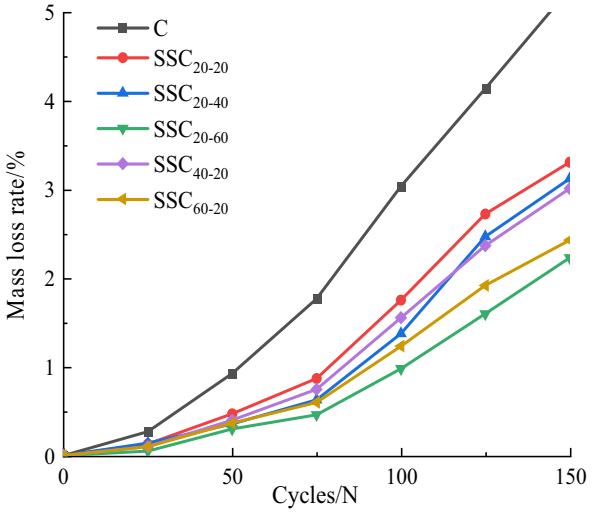


**Figure 8:** Relation between mass loss rate and freezing-thawing cycles.

the bearing capacity of concrete, the internal microcracks of concrete specimens result in gradual increases in the spalling amounts of cement mortar on the surface [40]. It was found that, after 150 freeze-thaw cycles, the mass loss rate of the OC reached a specified value of 5%, and the specimens were considered to have become damaged. The mass loss rates of the concrete with different dosages of SSA in descending order were as follows: 3.024% for $SSC_{20-20}$; 3.015% for $SSC_{40-20}$; 2.658% for $SSC_{20-40}$; 2.432% for $SSC_{60-20}$; and 2.233% for $SSC_{20-60}$. The reasons for these results were that SS could react to cement hydration and produce C–S–H gels and fill some pores; the number of pores was reduced and effectively prevented the flow of the aqueous solution, so that the hydrostatic pressure or osmotic pressure could be reduced [41], which resulted in the overall structure being stabler, thereby further reducing the degree of freeze-thaw damage in the SSC. Therefore, it could be ascertained from the experimental results that appropriate increases in the SS admixture could effectively reduce the mass loss rates of the SSC.

### 3.3.2 Relative dynamic modulus of elasticity analysis

The dynamic elastic modulus of the specimens was tested by DT-20W, and the dynamic elastic modulus of each cycle of each group of specimens was computed using formula (6).

$$\Delta E_n = \frac{E_0 - E_n}{E_0} \times 100\%, \tag{6}$$

where $E_0$ represents the dynamic modulus of concrete specimens before freezing-thawing cycles, $E_n$ indicates the dynamic modulus of concrete specimens after $N$ times of freezing-thawing cycles.

Figure 9 shows the fractional changes in the relative dynamic modulus of elasticity of the specimens following the freezing-thawing cycles. As the freeze-thaw tests progressed, the relative dynamic modulus of elasticity of the concrete exhibited varying degrees of decline, which indicated that the internal damages were gradually accumulating and intensifying. It was observed that when the number of freeze-thaw cycles reached 50, the internal damages to the specimens in each group were small, and the modulus of dynamic elasticity was maintained above 90%. The reason for this was that aqueous solution continuously entered the interior of concrete, and freezing-thawing occurred in the pores. When the expansion pressure produced by ice crystal exceeded

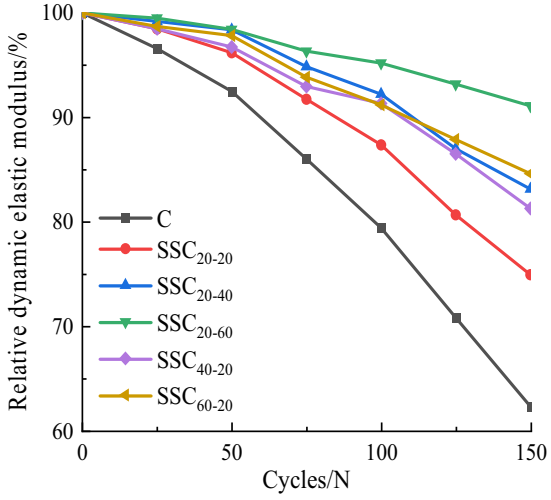


**Figure 9:** Relationship between relative dynamic elastic modulus and freezing-thawing cycles.

the force that the concrete could bear, the concrete would produce frost heave cracking and form some microcracks, thereby resulting in damage [42]. $SSC_{20-40}$ and $SSC_{20-60}$ showed the smallest decline in modulus of dynamic elasticity, with almost no change observed. The $SSC_{20-60}$ Group showed the slowest decline, indicating that the internal damages caused by the freezing-thawing conditions were also small. Then, after 150 freezing-thawing cycles, the modulus of elasticity decreased to 62.3%, which was close to the specified value of 60%, at which point the specimens were considered to be damaged. The main reason for these results was that the increase of freezing-thawing cycles and the repeated freezing-thawing of aqueous solution in the capillary of concrete led to the continuous extension and expansion of cracks, and finally to the mutual penetration of cracks, so that the concrete was seriously damaged [43]. However, the $SSC_{20-20}$ Group decreased to 74.92%, and the other SSC were more than 80%, indicating good performance in terms of frost resistance. This study determined that the decreases of the relative dynamic elastic modulus of SSC specimen groups were as follows: $SSC_{20-20}$: 25.08%; $SSC_{20-40}$: 16.88%; $SSC_{20-60}$: 8.91%; $SSC_{40-20}$: 18.73%; and $SSC_{60-20}$: 15.41%. The relative dynamic modulus of the SSC decreased with the increases in the freezing-thawing cycles. However, the relative dynamic modulus decreased less with the increase of SS content. The bonding interfaces of the SSA and the cement slurry were better than those of the ordinary aggregate and the cement slurry. Therefore, when the concrete specimens were at the same freezing-thawing damage degree, the cracking damages were smaller and the frost resistance was better.

**Table 7:** Damage calculation model

| | |
|---|---|
| Unary quadratic function | $E_\alpha/E_0 = aN^2 + bN + c$ |
| Exponential function | $E_\alpha/E_0 = ae^{bN}$ |

$E_\alpha/E_0$: The relative dynamic elastic modulus of concrete. $a$, $b$, $c$: the correlation coefficients.
$N$: The freezing-thawing cycle coefficient.

### 3.3.3 Freezing-thawing damage model and life prediction based on relative dynamic elastic modulus

In order to investigate the causes of the freezing-thawing damages to SSC, this study conducted an analysis based on the gradual accumulation of small internal damages using a damage mechanics theory as the basis. The freeze-thaw damage process could be expressed as follows: (1) Micro-cracks were generated within the concrete; (2) Macro-cracks appeared; and (3) Matrix damages occurred [44]. During the experimental tests, concrete cracking had occurred after water absorption resulting in increases in the masses of the specimens. The relative dynamic modulus of elasticity was used as a variable in order to respond to the degrees of freezing-thawing damage ($D$) to SSC. The equation was as follows:

$$D = 1 - \frac{E_\alpha}{E_0}. \tag{7}$$

In formula (7), $D$ denotes the degree of concrete damage; $E_0$ represents initial dynamic modulus; and $E_\alpha$ indicates dynamic modulus after freezing-thawing test. Based on the above equation and with reference to the literature [45,46], a quadratic and exponential function is chosen to express the freeze-thaw damage model; the models are depicted in Table 7.

The fitting results are shown in Tables 8 and 9. It can be seen from the tables that the fitting accuracy $R^2$ of the quadratic function was between 0.982 and 0.999. The fitting accuracy $R^2$ of the exponential function was between 0.926 and 0.960. Therefore, the quadratic function model was able to better reflect the freezing-thawing damage law of the SSC.

Figure 10 reveals the curve fitting of the relative dynamic elastic modulus of the quadratic function of the SSC. According to the model, the freeze-thaw cycles of the SSC could be calculated when the relative dynamic elastic modulus decreased to 60%. The results are detailed in Table 9. According to ref. [47], the annual average

**Table 8:** Results of fitting parameters of exponential function

| Test specimen number | $a$ | $b$ | $R^2$ |
|---|---|---|---|
| C | 1.02833 | $-2.94 \times 10^{-3}$ | 0.946 |
| $SSC_{20-20}$ | 1.0234 | $-1.84 \times 10^{-3}$ | 0.930 |
| $SSC_{20-40}$ | 1.01809 | $-1.25 \times 10^{-3}$ | 0.932 |
| $SSC_{20-60}$ | 1.00687 | $-6.19 \times 10^{-4}$ | 0.960 |
| $SSC_{40-20}$ | 1.01627 | $-1.31 \times 10^{-3}$ | 0.926 |
| $SSC_{60-20}$ | 1.01485 | $-1.09 \times 10^{-3}$ | 0.934 |

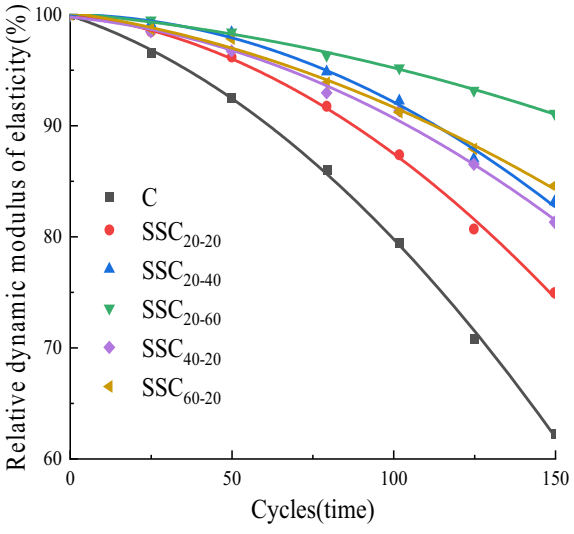


**Figure 10:** Fitting curves of relative dynamic elastic modulus and freezing-thawing cycles.

**Table 9:** Results of the fitted parameters of the quadratic function

| Test specimen number | $a$ | $b$ | $c$ | $R^2$ |
|---|---|---|---|---|
| C | $-9.58 \times 10^{-6}$ | $-1.090 \times 10^{-3}$ | 1.00074 | 0.999 |
| $SSC_{20-20}$ | $-8.63 \times 10^{-6}$ | $-3.869 \times 10^{-4}$ | 1.00070 | 0.999 |
| $SSC_{20-40}$ | $-5.36 \times 10^{-6}$ | $-3.744 \times 10^{-4}$ | 1.00398 | 0.982 |
| $SSC_{20-60}$ | $-2.51 \times 10^{-6}$ | $-2.225 \times 10^{-4}$ | 1.00037 | 0.999 |
| $SSC_{40-20}$ | $-6.79 \times 10^{-6}$ | $-2.133 \times 10^{-4}$ | 0.99873 | 0.998 |
| $SSC_{60-20}$ | $-5.52 \times 10^{-6}$ | $-2.076 \times 10^{-4}$ | 1.00062 | 0.999 |

**Table 10:** Number of frozen and melting circulation of concrete when the relative dynamic elastic modulus reached 60% ($N$)

| Specimen number | C | $SSC_{20-20}$ | $SSC_{20-40}$ | $SSC_{20-60}$ | $SSC_{40-20}$ | $SSC_{60-20}$ |
|---|---|---|---|---|---|---|
| Number of freezing-thawing cycles | 155 | 194 | 242 | 357 | 227 | 250 |

**Table 11:** Freezing-thawing cycle life of concrete when the relative dynamic elastic modulus reached 60% (years)

| Numbering | C | $SSC_{20-20}$ | $SSC_{20-40}$ | $SSC_{20-60}$ | $SSC_{40-20}$ | $SSC_{60-20}$ |
|---|---|---|---|---|---|---|
| North-east area | 10.3 | 12.9 | 16.1 | 23.8 | 15.1 | 16.7 |
| North-west region | 10.5 | 13.2 | 16.4 | 24.2 | 15.4 | 16.9 |
| North China | 14.8 | 18.5 | 23.0 | 34.0 | 21.6 | 23.8 |

numbers of freezing-thawing cycles in northern China are as follows: 84× in the north; 118× in the northwest; and 120× in the northeast.

After improving upon the lifespan prediction model of Vesikari [48], the relationship between freezing-thawing cycles and the service life is proposed. Then, after referring to a large number of data, the value of the conversion coefficient $k$ of the number of indoor and outdoor freezing and thawing cycles was summarized [49,50].

$$t = \frac{kN}{M}, \tag{8}$$

where $t$ represents the service life of concrete, $k$ indicates the rapid freezing-thawing coefficient in the laboratory, taken as 1:8 in this paper, *i.e.*, number of the freeze-thaw cycles indoor equivalent to 8× of the natural environment, $M$ indicates the number of freeze-thaw cycles that concrete structures may undergo in the natural environment, and $N$ indicates the number of freezing-thawing cycles of concrete when the relative dynamic elastic modulus is decreased to 60%.

According to the number of freeze-thaw cycles and prediction model of concrete in Table 10, the durability life of concrete in northern regions can be obtained, and the results are shown in Table 11.

In Table 11, the anti-freezing-thawing lifespans of different specimens were measured in years. The freezing-thawing lifespan of the SSC with different dosages in northern China had increased. The anti-freezing-thawing lifespans of the SSC were greatly improved when compared with those of the OC. The freezing-thawing lifespan of concrete in the Group $SSC_{20-60}$ was more than twice that of the OC. In addition, when compared with the OC, the freezing-thawing life durability of the SSC specimens had been greatly improved, which indicated that the incorporation of SS as an aggregate was an effective method for improving the anti-freezing-thawing durability of concrete.

# 4 Conclusion

(1) Appropriate increases in the amount of SSA could effectively improve the frost resistance of concrete, and the frost resistance of $SSC_{20-60}$ was superior to that of the other examined groups.
(2) The performance of OC and $SSC_{20-60}$ was analyzed in nanospace to research the damage mechanisms. It was concluded that the high density of SSC can effectively inhibit the aqueous solution into the concrete, thereby avoiding the damage to the concrete caused by the expansion pressure formed by the ice crystals. Therefore, $SSC_{20-60}$ exhibited better frost resistance durability.
(3) A freeze-thaw damage calculation model of SSC was established with the relative dynamic elastic modulus as the variable. It was found that the freezing-thawing durability lifespans of the $SSC_{20-60}$ and $SSC_{60-20}$ were longer, at 357 and 250 cycles, respectively. It was observed that after adding a certain amount of SS to the concrete specimens, the freezing-thawing durability lifespans were significantly improved when compared with OC.
(4) Combined with the average number of freeze-thaw times in northern China, the freeze-thaw durability of SSC was predicted according to the damage calculation model. It was concluded that SSC had better freeze-thaw durability, and the freeze-thaw cycle lifespan of $SSC_{20-60}$ was predicted to be longer than that of OC, at more than twice that of the OC. The results confirmed that the concrete prepared with SS as an

aggregate could achieve improved freezing-thawing durability, which provided a reference for the future application of SSC in practical engineering projects.

(5) A freezing-thawing damage calculation model was established in this study by using the relative dynamic elasticity as a variable. It was found that the accuracy of its correlation coefficient values could reach more than 0.982. Therefore, the model established in this study was considered to have significant reference value for the prediction of frost resistance durability lifespans of SSC in cold regions.

**Acknowledgements:** One of the authors (H. S.) is thankful to his teacher's help and guidance and thanks his girlfriend Wang Siqi's for encouragement and support.

**Funding information:** This study was funded by the National Natural Science Foundation of China (grant no. 51768056).

**Author contributions:** Manuscript writing and data analysis mainly completed by Hui SUN, all authors have accepted responsibility for the entire content of this manuscript and approved its submission.

**Conflict of interest:** The authors state no conflict of interest.

**Data availability statement:** All data, models, and code generated or used during the study appear in the submitted article.

# References

[1] USGS. Iron and steel slag statistics and information. Accessed 06/05/2015.
[2] Guo J, Bao Y, Wang M. Steel slag in China: treatment, recycling, and management. Waste Manag. 2018;78:318–30.
[3] Olofinnade O, Morawo A, Okedairo O, Kim B. Solid waste management in developing countries: Reusing of steel slag aggregate in eco-friendly interlocking concrete paving blocks production. Case Stud Constr Mater. 2021;14:e00532.
[4] Maslehuddin M, Sharif AM, Shameem M, Ibrahim M, Barry MS. Comparison of properties of steel slag and crushed limestone aggregate concretes. Constr Build Mater. 2003;17(2):105–12.
[5] Liuchunlin Zha, Kunpeng Chen. Depeng, possibility of concrete prepared with steel slag as fine and coarse aggregates: a preliminary study. Procedia Eng. 2011;4:412–6.
[6] Anastasiou E, Papayianni I. Criteria for the use of steel slag aggregate in concrete. M. S. Konsta-Gdoutos. Measuring, monitoring and modeling concrete properties. Netherlands: Springer; 2006. p. 419–26.
[7] Furlani E, Tonello G, Maschio S. Recycling of steel slag and glass cullet from energy saving lamps by fast firing production of ceramics. Waste Manag. 2010;30:1714–9.
[8] Wu W, Zhang W, Ma G. Optimum content of copper slag as a fine aggregate in high strength concrete. Mater Des. 2010;31:2878–83.
[9] Subathra Devi V, Gnanavel BK. Properties of concrete manufactured using steel slag. Procedia Eng. 2014;97:95–104.
[10] Chunlin L, Kunpeng Z, Depeng C. Possibility of concrete prepared with steel slag as fine and coarse aggregates: a preliminary study. Procedia Eng. 2011;24:412–6.
[11] Wang S, Zhang G, Wang B, Wu M. Mechanical strengths and durability properties of pervious concretes with blended steel slag and natural aggregate. J Clean Prod. 20 October 2020;271:122590.
[12] Fagerlund G. A service life model for internal frost damage in concrete, Div. Building materials, Lund Institute of Technology; 2004. Report TVBM-3119.
[13] Liu M, Wang Y. Damage constitutive model of fly ash concrete under freeze-thaw cycles. J Mater Civ Eng. 2012;24(9):1165–74.
[14] Duan A, Jin W, Qian J. Effect of freeze-thaw cycles on the stress-strain curves of unconfined and confined concrete. Mater Struct. 2011;44:1309–24.
[15] Duan A, Tian Y, Dai JG, Jin WL. A stochastic damage model for evaluating the internal deterioration of concrete due to freezing-thawing action. Mater Struct. 2014;47:1025–39.
[16] Penttala V. Surface and internal deterioration of concrete due to saline and non-saline freezing-thawing loads. Cem Concr Rer. 2006;36(5):921–8.
[17] Zhang X, Wang L, Zhang J. Mechanical behavior and chloride penetration of high strength concrete under freezing-thawing attack. Cold Reg Sci Technol. 2017;142:17–24.
[18] Cao DF, Fu LZ, Yang ZW. Test study on tensile properties of concrete after freezing-thawing cycles. J Buil Mater. 2012;15(1):48–52.
[19] Liu MH, Wang YF. Damage constitutive model of fly ash concrete under freeze-thaw cycles. J Mater Civ Eng. 2012;24(9):1165–74.
[20] Paolo F. Analytical model to predict the lifetime of concrete members externally reinforced with FRP. Theor Appl Fract Mec. 2015;75:137–45.
[21] Sun W, Zhang YM, Yan HD, Mu R. Damage and resistance of high strength concrete under the action of load and freezing-thawing cycle. Cem Concr Res. 1999;29:1519–23.
[22] Mason B. The constitution of some open-heart slag. J Iron steel Inst. 1994;11:69–80.
[23] Yu H, Ma H, Yan K. An equation for determining freeze-thaw fatigue damage in concrete and a model for predicting the service life. Constr Build Mater. 2017;137:104–16.
[24] Gao C, Shen XD, Wang XX. Freezing-thawing resistance of lightweight aggregate concrete with stress damage. J Chin Ceram Soc. 2014;42(10):1247–52.
[25] Chenxia W, Lu L, Fubo C, Lan L. Experimental study on mechanical properties of recycled concrete after freeze-thaw cycles. J Build Struct. 2020;41(12):193–202. (In Chinese).
[26] Meiyan H, Minghui J, Wenlei Z, Yubin Y, Teng C, Hao W. Composite salt corrosion deterioration characteristics and

damage calculation models of concrete incorporated with corrosion inhibiting admixtures. J Build Eng. 2021;44(1):103221.
[27] Ali K, Qureshi MI, Saleem S, Khan SU. Effect of waste electronic plastic and silica fume on mechanical properties and thermal performance of concrete. Constr Build Mater. 2021;285(11):122952.
[28] Qin XC, Meng SP, Cao DF, Tu YM, Sabourova N, Grip N. Evaluation of freezing-thawing damage on concrete material and prestressed concrete specimens. Constr Build Mater. 2016;125:892–904.
[29] Liu L, Wang XC, Zhou J, Chu HQ, Shen DJ, Chen HS, et al. Investigation of pore structure and mechanical property of cement paste subjected to the coupled action of freezing/thawing and calcium leaching. Cem Concr Res. 2018;109:133–46.
[30] Mehta PK, Monteiro PJ. Concrete: microstructure, properties and materials. 3rd edn. New York: McGraw-Hill; 2006.
[31] Pigeon M, Pleau R. Durability of concrete in cold climates. 1st edn. London: E&FNSPON; 1995.
[32] Wang B, Pan J, Fang R, Wang Q. Damage model of concrete subjected to coupling chemical attacks and freeze-thaw cycles in saline soil area. Constr Build Mater. 2020 May 10;242:118205.
[33] Liu CH, Wan JP. Probability theory and mathematical statistics. Beijing: Higher Education Press; 2001 (In Chinese).
[34] Fan XC, Wu D, Chen H. Experimental research on the freezing-thawing resistance of basalt fiber reinforced concrete. Adv Mat Res. 2014;919–921:1912–5.
[35] Guo K, Ma HH, Yang FS, Zhao TY. Micromechanical properties of GO-RC interface transition zone under Freeze-Thaw cycle. J Build Mater. 2020;1(23):230–8 (In Chinese).
[36] Chen JX, Deng XH, Luo YB, He LC, Liu Q, Qiao X. Investigation of microstructural damage in shotcrete under a freeze–thaw environment. Constr Build Mater. 2015;83:275–82.
[37] Bullard JW, Jennings HM, Livingston RA, Nonat A, Scherer GW, Schweitzer JS, et al. Mechanisms of cement hydration. Cem Concr Res. 2011;41(12):1208–23.
[38] Powers TC. A working hypothesis for further studies of frost resistance. J Am Concr Inst. 1945;16(4):245–72.
[39] Wang BX, Wang F, Wang Q. Damage constitutive models of concrete under the coupling action of freezing-thawing cycles and load based on Lemaitre assumption. Constr Build Mater. 2018;173:332–41.
[40] Hang MY, Cui L, Wu JQ, Sun ZK. Freezing-thawing damage characteristics and calculation models of aerated concrete. J Build Eng. 2020;28:101072.
[41] Li B, Mao JZ, Shen WG, Liu HB, Liu XZ, Xu GL. Mesoscopic cracking model of cement-based materials subjected to freeze-thaw cycles. Constr Build Mater. 2019;211:1050–64.
[42] Powers TC. Resistance to weathering-freezing and thawing. Portland Cement Assoc R&D Lab Bull; 1900.
[43] Qiu J, Zhou Y, Vatin NI, Guan X, Sultanov S, Khemarak K. Damage constitutive model of coal gangue concrete under freeze-thaw cycles. Constr Build Mater. 20 December 2020;264:120720.
[44] Fu YW, Cai LC, Cao DG. Study on freeze thaw durability and damage model of alkali activated slag high performance concrete. Eng Mech. 2012;23(3):103–9 (In Chinese).
[45] Liu L, Xu SX, Chen HS, Zhao HT. Numerical investigation of the effects of freezing on micro-internal damage and macro-mechanical properties of cement pastes. Cold Reg Sci Technol. 2014;106–107(10):141–52.
[46] Niu JG, Zuo FL, Wang JL. Freeze thaw damage model of plastic steel fiber reinforced lightweight aggregate concrete. J Build Mater. 2018;21(2):235–40 (In Chinese).
[47] Zhang RF, Wang X, Fan HM, Zhou LL, Wu M, Liu YH. Study on the division of freezing-thawing zones and the characteristics of zoning erosion in China. Sci Soil Water Conserv China. 2009;7(2):24–8 (In Chinese).
[48] Vesikari E. Service life design of concrete structures with regard to the frost resistance of concrete. Nordic Concr Res. 1986;5:215–28.
[49] Li J, Peng XP, Deng ZG. Quantitative design on the frost resistance of concrete. Concrete. 2000;12:61–5. (In Chinese).
[50] Wu HR, Jin WL, Yan YD. Freeze thaw environment zoning and frost resistance life prediction of concrete. J Zhejiang Univ (Eng edn). 2012;46(4):650–7 (In Chinese).